Geophys. Astrophys. Fluid Dynamics, 1987, Vol. 37, pp. 253–278
0309-1929/87/3704-0253 $18.50/0

Printed in Great Britain

Open-Ocean Response and Normal Mode Excitation in an Eddy-Resolving General Circulation Model

ARTHUR J. MILLER

Scripps Institution of Oceanography, IGPP A-025, La Jolla, CA 92093, U.S.A.

WILLIAM R. HOLLAND

The National Center for Atmospheric Research, Boulder, CO 80307, U.S.A.

and

MYRL C. HENDERSHOTT

Scripps Institution of Oceanography, IGPP A-025, La Jolla, CA 92093, U.S.A.

(*Received June 17, 1986*)

Analysis of a two-layer, flat-bottom, steady-wind driven, eddy-resolving general circulation model reveals a distinct separation in frequency of baroclinic and barotropic motion in the region distant from the model Gulf Stream. The far-field motions at periods less (greater) than about 100 days are predominantly barotropic (baroclinic), unlike the near-field, eddy-generating, free-jet region which contains barotropic and baroclinic energy throughout the model frequency range. The far-field barotropic energy produces a peak in the model sea-level spectra between 25 and 50 days with a magnitude comparable to energy levels observed in spectra of sea level from oceanic island tide gauges. The far-field barotropic motion is clearly composed of large-scale, resonant, barotropic normal modes drive by mesoscale activity of the turbulent, free-jet region. Oceanic mesoscale turbulence may therefore provide for planetary normal modes an excitation mechanism distinct from atmospheric forcing.

The open-ocean, barotropic, model response is very similar to that of a fluctuating-wind driven model, which suggests that atmospheric and intrinsic forcing of mid-ocean eddies may be of comparable importance.

KEY WORDS: Ocean Circulation, mesoscale currents, quasigeostrophic flows, Rossby waves.

1. INTRODUCTION

Open-ocean mesoscale eddies have been discussed extensively (Robinson, 1983). The energy sources believed to be important in their maintenance fall into two basic classes: atmospheric forcing (primarily through wind stress) and intrinsic forcing (primarily through oceanic instabilities). The relative importance of these mechanisms is uncertain (Wunsch, 1981; Muller, 1983). The resolution of this uncertainty has important consequences for oceanic general circulation theory.

Atmospheric forcing of oceanic transients has been theoretically examined by Muller and Frankignoul (1981) and by Willebrand *et al.* (1980). These studies predicted and observed insignificant local coherence between atmospheric and oceanic variables for periods between about 10 and 100 days and strong coherence for shorter periods. Model kinetic energy and vertical displacement response spectra were comparable in magnitude to observed spectra. Both studies therefore concluded that direct atmospheric forcing may be the dominant driving mechanism for mid-ocean eddies.

Mechanisms for the intrinsic generation of fluctuations include open-ocean instability (Gill *et al.*, 1974; Robinson and McWilliams, 1974), radiation of Rossby waves from Gulf Stream rings (Flierl *et al.*, 1975; Flierl, 1977), boundary current radiation (Pedlosky, 1977; Harrison and Robinson, 1979; Talley, 1983a, b) and topographic interaction (Bretherton and Karweit, 1975; Rhines, 1977). Linear analytical studies have had limited success with predicting mid-ocean spectral levels because of the essentially nonlinear nature of fully developed instabilities of ocean currents. The treatment of nonlinear phenomena, particularly time-dependent ones, is analytically unwieldy. For this reason, numerical integrations of nonlinear flows have been extremely useful in developing an understanding of the influence of instabilities in the ocean (for a review see Holland *et al.*,

1983). In particular, eddy-resolving general circulation models (EGCMs) in bounded domains can allow strong currents to develop and become unstable, producing a variety of time-dependent mesoscale structures such as "Gulf Stream"-like free jets, Ring-like vortices, Rossby waves and eddies.

In this study, we wish to determine to what extent an EGCM may produce an open-ocean response similar to observations. We examine the far-field response of the large basin (4000 km square), quasigeostrophic, two-layer, flat-bottom EGCM solution of Schmitz and Holland (1982). The wind forcing is steady so that all transients arise solely from the intrinsic instabilities of the system. Previous analyses of EGCMs (e.g. Harrison and Robinson, 1978; Holland and Rhines, 1980; Harrison and Holland, 1981) have concentrated on mean and eddy velocity fields in the model Gulf Stream region. We choose to concentrate on mid-ocean sea-level fluctuations since these ultimately may be compared to the observational data base of island tide-gauge records of the Pacific Ocean (Luther, private communication).

The far-field sea-level response of this EGCM is found to be comparable to typical, observed, mid-ocean sea-level spectra in the 25–50 day period band. The turbulent region near the model Gulf Stream acts as a broadband localized energy source which strongly radiates into this band. Model-ocean frequency spectra far from the source region unexpectedly resemble the frequency-response curves of Phillips' (1966) deterministic model of fluctuating-wind-forced flow in closed basins and are evidently similarly controlled in shape and amplitude by the dissipative parameterization (Harrison, 1979). Moreover, the interior response of this EGCM is remarkably similar to the model response of Willebrand *et al.* (1980) which was forced by stochastic, inhomogeneous winds. Linear normal mode decomposition of the large-scale barotropic response of the present model shows that it is composed of resonant barotropic basin modes driven by western basin turbulence and damped by bottom friction.

The following section discusses the quasigeostrophic model utilized in this study. In Section 3, we examine the time-dependence of the model response (cf. Schmitz and Holland, 1982) in terms of sea-level fluctuations. Section 4 describes the barotropic normal mode decomposition and analysis. A discussion of the results and conclusions are presented in Sections 5 and 6, respectively.

2. QUASIGEOSTROPHIC MODEL

Oceanic motions with time scales longer than a few days and length scales greater than a few tens of kilometers are often approximated by the quasigeostrophic (QG) equations (Pedlosky, 1979, Ch. 6). High resolution, finite difference versions of these equations have been numerically integrated by Holland (1978) and others. In this study, we employ the 4000 km square basin, two-layer, QG model (Experiment 5.13) discussed by Schmitz and Holland (1982).

The fully nonlinear QG potential vorticity equations in standard form are

$$D_1 Q_1/Dt = F_1 + H_1^{-1} \nabla \times \tau, \tag{2.1a}$$

$$D_3 Q_3/Dt = F_3 + B_3, \tag{2.1b}$$

where

$$Q_1 = \nabla^2 \psi_1 + \beta y - (f_0^2/g' H_1)(\psi_1 - \psi_3), \tag{2.2a}$$

$$Q_3 = \nabla^2 \psi_3 + \beta y + (f_0^2/g' H_3)(\psi_1 - \psi_3) + (f_0/H_3)h. \tag{2.2b}$$

In each layer the potential vorticity, Q, is conserved following fluid parcels except for the effects of dissipation (F and B) and forcing ($\nabla \times \tau$). Dissipative effects are modeled as Ekman friction,

$$B_3 = -\varepsilon \nabla^2 \psi_3, \tag{2.3}$$

in the lower layer and biharmonic friction,

$$F_i = -A \nabla^6 \psi_i, \qquad (i = 1, 3), \tag{2.4}$$

in each layer. The model was forced by a steady, double-gyre wind pattern (Figure 1c). Notation is summarized in Figure 1; further details are given by Schmitz and Holland (1982).

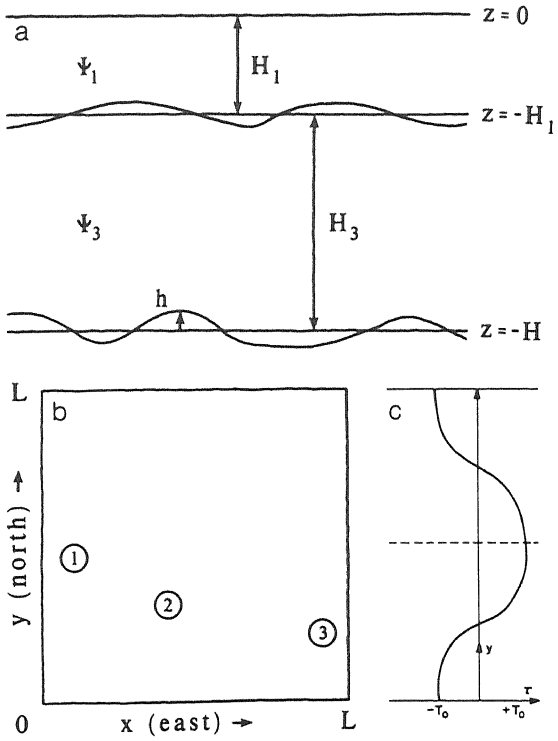

FIGURE 1 Vertical geometry of the quasigeostrophic model. The velocity streamfunctions, ψ_i, in each layer satisfy (2.1) with $D_i \cdot /Dt \equiv \partial_t + J(\psi_i, \cdot)$, $J(A,B) \equiv -\partial_y A \partial_x B + \partial_x A \partial_y B$, $\nabla^2 \equiv \partial_x^2 + \partial_y^2$, the Coriolis frequency $f \equiv f_0 + \beta y$, $g' \equiv g\Delta\rho/\rho_0$, $g \equiv$ gravitational acceleration, $\Delta\rho \equiv$ density jump across layer interface, $\rho_0 \equiv$ mean density with $\Delta\rho \ll \rho_0$, $H_i \equiv$ mean depth of each layer, $H \equiv H_1 + H_3$, $H' \equiv H_1^{-1} + H_3^{-1}$, $h \equiv$ topographic deviation from constant depth. Parameter values are $f_0 = 9.3 \times 10^{-5}\,\text{sec}^{-1}$, $\beta = 2.0 \times 10^{-11}\,\text{m}^{-1}\,\text{s}^{-1}$, $g' = 0.02\,\text{m}\,\text{s}^{-2}$, $\varepsilon = 1 \times 10^{7}\,\text{s}^{-1}$, $A = 8 \times 10^{9}\,\text{m}^4\,\text{s}^{-1}$, $H_1 = 1000\,\text{m}$ and $H_3 = 4000\,\text{m}$. (b) Horizontal geometry of the basin with $L = 4000\,\text{km}$. The numbers indicate the locations of simulated island tide-gauge stations. (c) The double-gyre, steady, wind stress forcing pattern. Here $\tau \equiv -\tau_0 \cos(\pi y/L)$, with $\tau_0 = 1 \times 10^{-4}\,\text{m}^2\,\text{s}^{-2}$.

It is convenient to discuss the model response in terms of a barotropic and baroclinic mode defined, respectively, to be

$$\psi \equiv (H_1\psi_1 + H_3\psi_3)/H, \qquad \phi \equiv \psi_1 - \psi_3. \tag{2.5a, b}$$

The barotropic mode is of particular interest. Equations governing

these two vertical modes are

$$\partial(\nabla^2\psi)/\partial t+\beta\psi_x+f_0H^{-1}J(\psi,h)+J(\psi,\nabla^2\psi)$$
$$=-\varepsilon H_3H^{-1}\nabla^2\psi+A\nabla^4\psi+H^{-1}\nabla\times\tau$$
$$+H_1H_3H^{-2}\{\varepsilon\nabla^2\phi+f_0H_3^{-1}J(\phi,h)-J(\phi,\nabla^2\phi)\}, \tag{2.6a}$$

$$(\partial/\partial t)[\nabla^2\phi-(f_0^2/g'H')\phi]+\beta\phi_x+(f_0H_1/HH_3)J(\phi,h)$$
$$+(H_3^2-H_1^2)H^{-2}J(\phi,\nabla^2\phi)$$
$$=-\varepsilon H_1H^{-1}\nabla^2\phi+A\nabla^4\phi+H_1^{-1}\nabla\times\tau$$
$$+\{\varepsilon\nabla^2\psi+f_0H_3^{-1}J(\psi,h)-J(\psi,\nabla^2\phi-[f_0^2/g'H']\phi)-J(\phi,\nabla^2\psi)\}. \tag{2.6b}$$

The terms which couple the two modes appear in curly brackets; they decouple only in the absence of nonlinearity, topography, and bottom friction. Topography is excluded from this study. (See the discussion section and Miller (1986a) for remarks on the inclusion of topography.)

Holland (1978) discusses the numerical schemes employed when integrating (2.1). The model was spun-up to a statistical steady state as determined from the time history of basin-integrated energetics (cf. Holland and Rhines, 1980). Six years of statistically equilibrated data was available. For reference, the time-averaged streamfunctions, $\bar{\psi}_1$, $\bar{\psi}_3$ and $\bar{\psi}$, are plotted in Figure 2a-c. As remarked by Schmitz and Holland (1982), the model Gulf Stream penetrates only about 1/5 the distance to the eastern boundary. Compact, recirculating gyres, typical of these simulations (Holland, 1978), are observed in the lower layer, north and south of the jet. Away from this region, the upper layer mean circulation is predominantly Sverdrup flow (cf. Holland and Rhines, 1980) and the lower layer is nearly motionless on average.

3. SEA-LEVEL VARIANCE

In this section we discuss in detail our analysis of model fluctuations

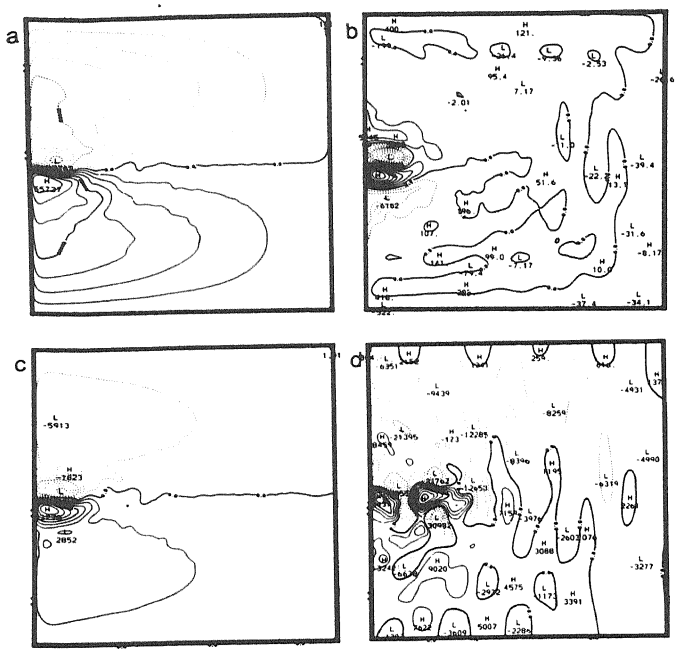

FIGURE 2 Streamfunction maps. (a) Mean ψ_1 (Contour Interval = $7000\,m^2\,s^{-1}$), (b) Mean ψ_3 (CI = $2000\,m^2\,s^{-1}$), (c) Mean barotropic ψ from (2.5a) (CI = $3000\,m^2\,s^{-1}$), (d) Instantaneous barotropic ψ (CI = $5000\,m^2\,s^{-1}$).

in the ocean interior, the "far-field" regions removed from strong mean currents. We have particular interest in the long, barotropic planetary waves, for which the best observational data are island tide-gauge records [see, for example, Rhines (1977) p. 227]. We therefore emphasize sea-level spectra such as would be observed by tide gauges on islands. Moreover, in the Pacific Ocean, island tide-gauge stations have a wide geographic distribution in contrast to typical current meter mooring arrays from which energy spectra are obtained. Therefore our approach affords the opportunity for exploring large-scale trends in spectral features. Also, the record lengths for tide gauges are usually much longer than moorings, so that low-frequency spectral estimates based on tide-gauge data have greater statistical reliability.

A picture of instantaneous barotropic flow is shown in Figure 2d. Perhaps the most conspicuous features of the far-field flow are the "banana-shaped" eddies characteristic of Rossby waves radiating

from a source region (Rhines, 1977; Haidvogel and Rhines, 1983). In this case, the source region appears to be the nonlinear, unstable region surrounding the free jet. An inspection of sea-level spectra at various locations in the basin will help us reveal the nature of this flow field. We define true sea level (TSL) to be

$$\eta \equiv f_0 \psi_1 / g, \tag{3.1}$$

where ψ_1 is the upper-layer streamfunction of the geostrophically-balanced flow. This is the sea level which would be observed on an island in a two-layer ocean. We define barotropic sea level (BSL) to be

$$\zeta \equiv f_0 \psi / g, \tag{3.2}$$

where ψ is the barotropic streamfunction. Note that since the upper-layer streamfunction,

$$\psi_1 = \psi + H_3 H^{-1} \phi, \tag{3.3}$$

it is evident that TSL is comprised of BSL plus a scaled baroclinic sea-level signal.

Consider the three locations marked in the basin of Figure 1b. Station 1 is in the intense eddy region, station 2 in the central ocean and station 3 near the eastern boundary. The BSL and TSL spectra are shown for these locations in Figure 3. (For completeness, and for possible comparison with future open-ocean current measurements, we present the corresponding zonal and meridional velocity spectra for the top and bottom layers in Figures 4 and 5, respectively.) In the intense eddy region (Figure 3a, d), TSL exceeds BSL at all frequencies and both spectra are predominantly red, which is indicative of strong nonlinear activity. In the central basin (Figure 3b, e), the low-frequency spectral content drops substantially for both TSL and BSL, leaving a broad peak centered near 0.025 cpd. In the eastern basin (Figure 3c, f), spectral levels drop further but most precipitously in the 0.007–0.02 cpd band (50–150 days). The resultant far-field TSL spectra (Figure 3c) are described typically by a broad-band peak centered at a period near 40 days, a low-frequency peak at periods longer than about 150 days, and a spectral gap separating these two peaks. We also note the presence of high-frequency, narrow-band peaks (e.g. at 0.078 cpd) which will subsequently be

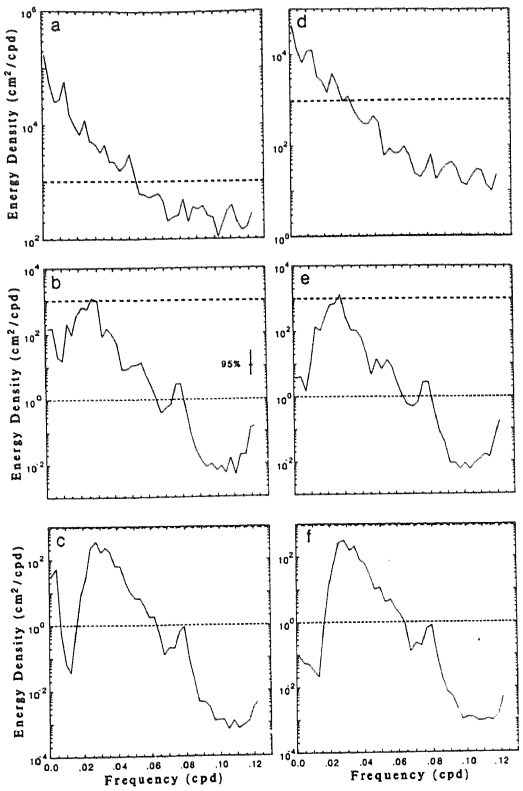

FIGURE 3 Sea-level spectra. (a-c) True sea level (TSL) as in (3.1). (d-f) Barotropic sea level (BSL) as in (3.2). Locations of stations are marked in Figure 1b. (a, d) are for station 1, in the turbulent Gulf Stream region, (b, e) are for station 2, in the central ocean, and (c, f) are from station 3, in the eastern basin. For comparison between plots, 10^0 is marked by a thin dashed line and 10^3 by a heavy dashed line. The 95% confidence interval (12 degrees of freedom) is the same for each plot and is indicated in (b).

identified with individual barotropic basin mode resonances.

Comparing the TSL to BSL spectra reveals an interesting feature. At stations 2 and 3, the spectra are nearly identical for frequencies greater than about 0.01 cpd (compare Figures 3b, c with 3e, f). Using (3.3) we can thus identify the high-frequency (periods $\lesssim$ 100 days) components of the far-field flow as nearly purely barotropic, in concert with Willebrand *et al.* (1980). Below about 0.01 cpd, the BSL spectra are orders of magnitude lower in power than TSL. This identifies the low-frequency content of the far-field response as nearly

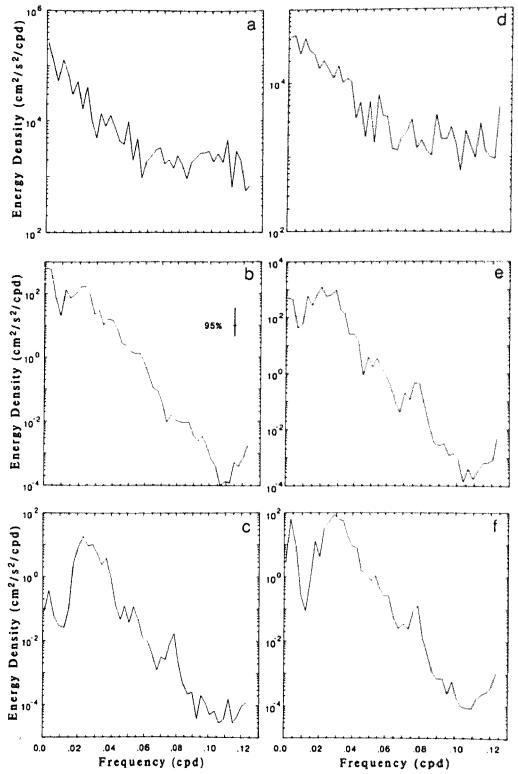

FIGURE 4 Upper-layer velocity spectra. (a-c) Zonal velocity. (d-f) Meridional velocity. Locations of stations as in Figure 3. The 95% confidence interval (8 degrees of freedom) is the same for each plot and is indicated in (b).

purely baroclinic flow. In contrast to the interior region, spectra from station 1 contain barotropic and baroclinic components at all frequencies (compare Figure 3a with 3d).

The far-field TSL spectra suggest frequency bands of differing physics. We consider four frequency bands: (i) the dominantly baroclinic band, (ii) the spectral gap, (iii) the dominantly barotropic broadband peak, and (iv) the high-frequency barotropic band. These bands correspond to (i) 0.0–0.005 cpd (2 yrs to 200 days), (ii) 0.005–0.017 cpd (200 days to 60 days), (iii) 0.017–0.05 cpd (60 days to 20 days), and (iv) 0.05–0.012 cpd (20 days to 8 days). Basin-wide maps

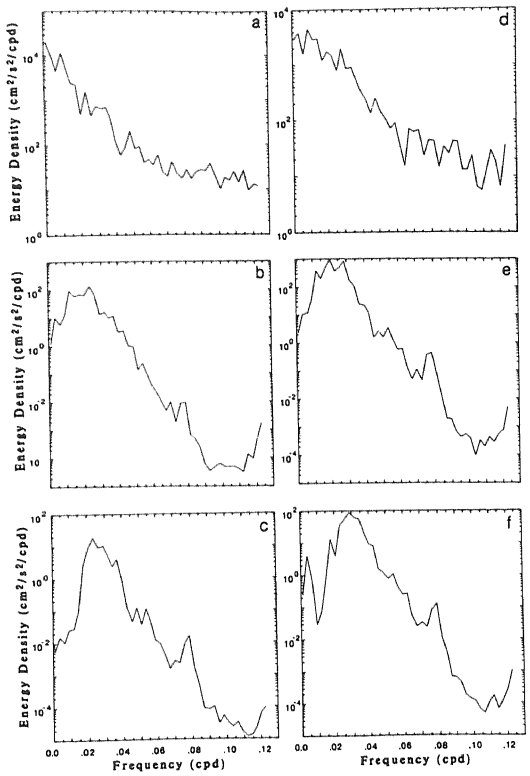

FIGURE 5 Same as Figure 4 but for lower-layer velocity components.

of the spectral amplitudes in these bands reveal some interesting features. We define sea-level variance to be

$$V \equiv \int_{f_1}^{f_2} F(f)\, df \tag{3.4}$$

where $F(f)$ is sea-level energy density and f_1 to f_2 delimits the frequency band of interest. Figure 6 shows TSL variance mapped to 100 km resolution for the four bands of interest. The rms amplitude of the fluctuations in a band at any location is simply $V^{1/2}$ cm. Note that this separation into bands will not be relevant to the dynamics

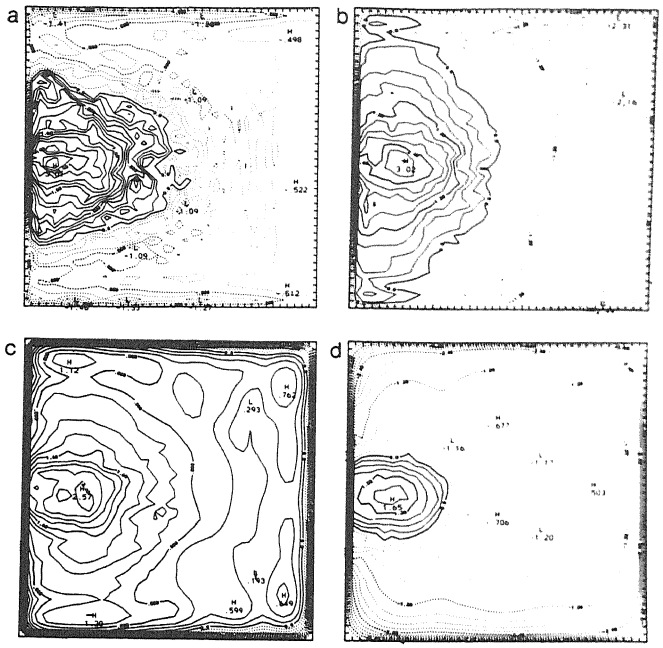

FIGURE 6 Basin-wide maps of sea-level variance, V, from (3.4). Contoured is $\log_{10} V$. Positive values are solid lines, negative values dashed. (a) The baroclinic band: period 2 yrs–200 days, (CI = 0.2 cm^2), (b) the spectral gap band: 200–60 days, (CI = 0.3 cm^2), (c) the barotropic broadband peak: 60–20 days, (CI = 0.2 cm^2), (d) the high-frequency, barotropic band: 20–8 days, (CI = 0.3 cm^2). The rms amplitude for waves in a given band is $V^{1/2}$ cm.

in the intense eddy region where nonlinear interactions may rapidly transfer energy between these frequency bands.

Variance levels in the lowest frequencies (baroclinic far field) nearly isotropically drop 2–3 orders of magnitude from the free-jet region to the interior ($\approx$2000 km away) where they level off (Figure 6a). The relatively uniform far-field response is substantially lower than that which is typically observed at these frequencies in oceanic tide-gauge spectra (see Section 5d). In the gap band, variance levels drop 4–5 orders of magnitude across the basin to the east (Figure 6b). This is indicative of a response trapped near the western boundary, virtually evanescent eastwards. In the barotropic far field (Figure 6c), the sea-level variance drops only about 1–2

orders of magnitude across the basin. There is some preference for stronger levels to the north and south. Variance levels in this band are very near to values observed in the Pacific and Atlantic mid-ocean (see Section 5d). The high-frequency band (Figure 6d) reveals structures of basin scale, which we present as further evidence of basin mode excitation which will be more fully discussed in the following section.

4. NORMAL MODE EXCITATION

The far-field response for the QG model has been shown to be barotropic for high frequencies ($f \gtrsim 0.01$ cpd) and baroclinic for low frequencies ($f \lesssim 0.01$ cpd). This suggests that the vertical modes decouple in the open ocean, away from the strong currents. The relatively low amplitude of these fluctuations suggests that they are driven by radiation from the high amplitude activity of the free-jet region. The far-field barotropic fluctuations will now be shown to consist of a superposition of resonant Rossby basin modes.

If we linearize (2.6a), ignore viscous effects, forcing and baroclinic topographic coupling, the equation for the barotropic flow becomes

$$\partial(\nabla^2\psi)/\partial t + J(\psi, \beta y + f_0 h H^{-1}) = 0, \tag{4.1}$$

with $\psi = 0$ on the boundary. The assumption of harmonic time dependence, $\psi = \exp(i\sigma_n t)\psi_n(x, y)$, yields an eigenproblem in the frequency, σ_n (eigenvalue), and streamfunction, ψ_n (eigenfunction). The solutions to (4.1) appear in conjugate pairs

$$(\sigma_n, \psi_n), \qquad (-\sigma_n, \psi_n^*),$$

where the asterisk indicates complex conjugation. The real part of either conjugate mode represents the same physical free mode. Owing to the self-adjoint linear operator of (4.1), the eigensolutions (together, in general, with the steady geostrophic mode) form a complete set of basis functions for QG motion in the basin.

One may represent a flow field as a summation of basin modes,

$$\psi(x, y, t) = \sum_n [a_n(t)\psi_n(x, y) + b_n(t)\psi_n^*(x, y)], \tag{4.2}$$

where the a_n and b_n are unique, time-dependent coefficients. Using the orthogonality relations (Rhines and Bretherton, 1973; Miller, 1986a),

$$\iint_{\text{basin}} \psi_n J(\psi_m^*, \beta y + f_0 h H^{-1})\, dx\, dy = \delta_{nm}, \tag{4.3a}$$

$$\iint_{\text{basin}} \psi_n J(\psi_m, \beta y + f_0 h H^{-1})\, dx\, dy = 0, \tag{4.3b}$$

we can solve for the modal coefficients,

$$a_n(t) = \iint_{\text{basin}} \psi J(\psi_n^*, \beta y + f_0 h H^{-1})\, dx\, dy, \tag{4.4}$$

where $b_n = a_n^*$ to insure the reality of the streamfunction field.

The flat-bottom ($h=0$) normal mode solutions are well known (Pedlosky, 1979, p. 147),

$$\psi_{nm} = \exp(i\beta x/2\sigma_{nm}) \sin(n\pi x/L) \sin(m\pi y/L), \tag{4.5a}$$

$$\sigma_{nm} = \beta/2\pi L^{-1}(n^2 + m^2)^{1/2}, \tag{4.5b}$$

where L is the basin width and n, m are positive integers. An example of a flat-bottom mode is shown in Figure 7. The familiar structure of a travelling wave of wavenumber $k = \beta/2\sigma_{nm}$ modulated by a space-dependent envelope is evident. We reference the modes by mode number, arranged in order of decreasing frequency, or equivalently by the values of (n, m). (Note that some flat-bottom modes are analytically degenerate for this square basin case, viz. modes (n, m) and (m, n) have the same frequency. We order these such that (n, m) precedes (m, n) where $(n < m.)$

The time-dependent complex coefficients of the 50 fastest (highest frequency, largest scale) flat-bottom modes were computed for the numerical model of Section 2. The Fourier spectrum of each coefficient's time series (with mean removed and a 10% cosine window applied) was computed. As a typical example of the response for an individual mode, Figure 8 shows the result for mode (2, 1), period 12.8 days. The spectrum is characterized by a strong, narrow peak very near the linear, intrinsic frequency of the mode. The peak extends above a background which is red for both positive

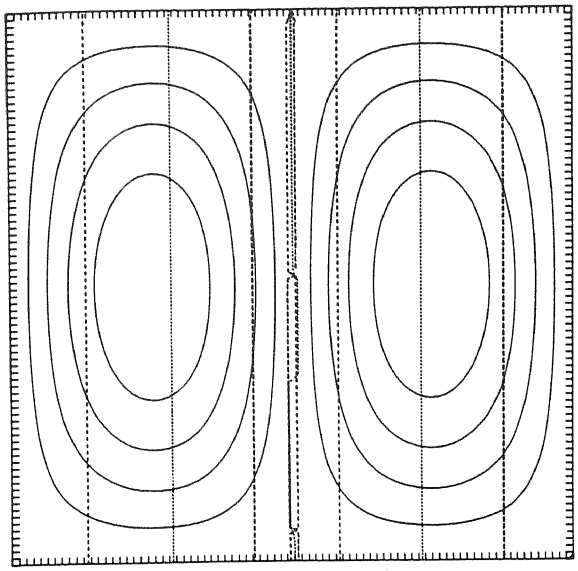

FIGURE 7 An example of the spatial structure of a flat-bottom Rossby mode. Plotted is mode 3, or mode (2, 1), with linear, intrinsic period 12.8 days. Solid lines are constant amplitude in 0.2 intervals, dashed lines are constant phase in $\pi/3$ intervals.

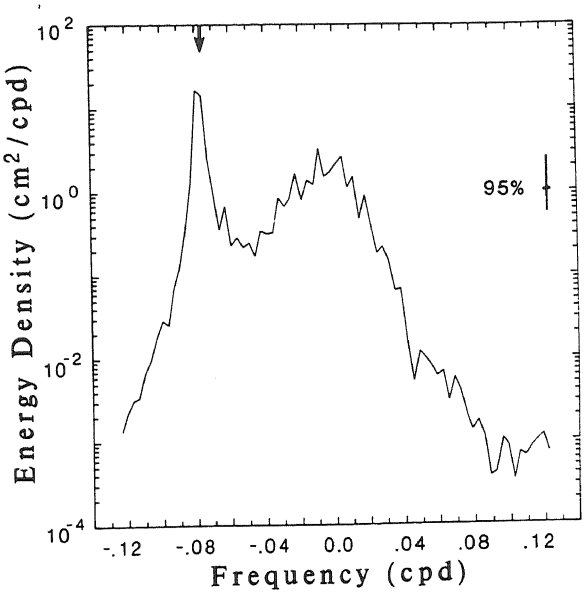

FIGURE 8 Power spectrum of the complex amplitude $a_3(t)$ of the complex normal mode $\psi_3^*(x, y)$. The spatial structure of ψ_3 is mapped in Figure 7. The mean was removed and a 10% cosine window was applied. The Fourier coefficients were averaged over 7 bins, and the 95% confidence interval (14 degrees of freedom) is indicated. The linear resonant frequency (period = 12.8 days) is marked with the arrow. Note the strongly resonant response for high frequencies and the broad peak near zero frequency. The rms amplitude of the observable mode is ≈ 0.23 cm. Lower-frequency modal spectra have peaks which rise even higher above the red background.

and negative frequencies and which culminates in a broad peak centered near zero frequency. The spectra of lower-frequency modes are similar although their resonant peaks typically rise much higher relative to the near-zero frequency peaks. The resonant peak is clearly the dominant feature of an individual normal mode response. Considering the nonlinearities of the western basin and the presence of mean currents, the strong excitation of the linear modes at resonance, even at mesoscale time scales, is surprising.

The time series of mode coefficients offer another perspective of model response. Figure 9 depicts time series of the real part of the complex amplitudes of representative modes. One can clearly see the dominant high-frequency oscillation of individual modes. An expanded view (not shown) reveals the lower-frequency activity associated with the broad peaks near zero frequency. The time series indicate sporadic excitation at resonance, occasionally punctuated by periods of weak activity. Individually, the time series resemble the responses of stochastically forced, resonant, linear oscillators.

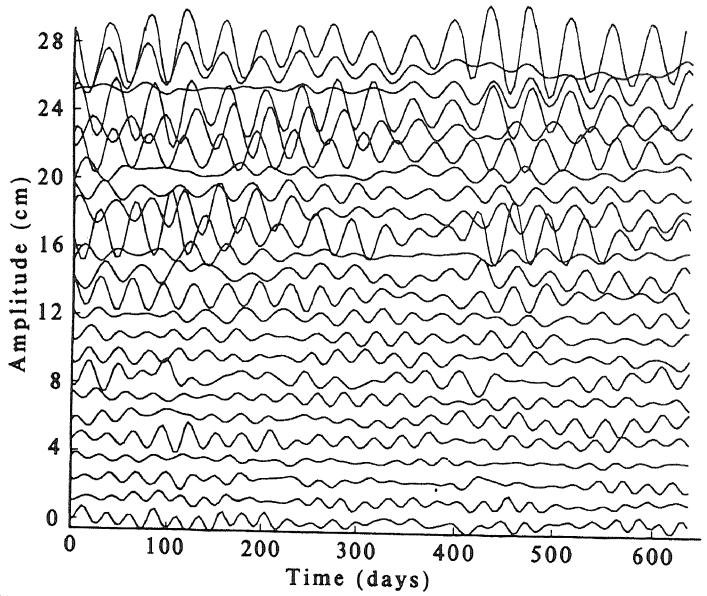

FIGURE 9 Time series of $\mathrm{Re}\{a_n(t)\}$ for modes 10 through 33 (from bottom to top), each offset by a constant value. Mode 10 (4, 1) has an intrinsic period of 23.8 days.

Factors that limit the resonant response of these modes are friction and nonlinearities (Pedlosky, 1965, 1967). Inspection of modal spectral resonant peak widths can give an indication of which effect is dominant. If the response is limited by bottom friction, the frequency bandwidth at the half-power point of the peak is

$$\delta f = r/\pi, \tag{4.6}$$

where $r \equiv \varepsilon H_3/H$ is the bottom friction parameter for the barotropic mode from (2.6a). (Biharmonic friction is insignificant for these large-scale waves.) If there are significant nonlinear effects, we expect the bandwidth to be broader. The value of r used in the numerical model sets $\delta f = 0.002$ cpd, which is a very narrow bandwidth. In order to resolve such a narrow peak, only minimal frequency band averaging can be performed with the record lengths available for this case. Most of the peaks are in fact so narrow that bottom friction alone can account for all the broadening. The nonlinearities acting on the basin-scale barotropic waves in this model appear to be only a mechanism for excitation.

5. DISCUSSION

(a) Rossby mode excitation

The original intent of this study was to explore the effects of exciting a linear Rossby mode at resonance in a highly turbulent quasi-geostrophic ocean. We sought to determine how much dissipation could be explained by nonlinear transfers to mesoscale eddies from a basin-scale mode with a similar time scale. After our initial modal decomposition of the two-layer, flat-bottom, QG simulation of Schmitz and Holland (1982), it became apparent that the reverse was occurring. The mesoscale turbulence had in fact *excited* a large number of basin modes at resonance. The finding of so much large-scale, wavelike behavior throughout the basin in the presence of mean currents, shear flows and mesoscale eddies was surprising and intriguing. The model suggests that western boundary region QG turbulence may provide for basin modes an excitation mechanism distinct from atmospheric forcing.

Published figures and diagnostics of other flat-bottom EGCMs (e.g. Holland, 1978; Robinson *et al.*, 1977) reveal many signs of resonant modes. For example, Holland's (1978) Figure 5 shows a strong resonance of the 64 day period, (2,2) planetary mode. The energy spectra (his Figure 9) also reveal this fundamental frequency and its higher harmonics [or, perhaps, a more weakly excited 32 day period, (1,1) mode].

The presence of topography may be expected to strongly modify these results. Topographic effects in EGCMs have not been fully explored, but the interruption of the flux of planetary-wave energy by topography is well known (Rhines and Bretherton, 1973; Rhines, 1977). To qualitatively assess the sensitivity of our results to variable relief, we have also analyzed several other EGCM cases (Chow, private communication) and decomposed them in terms of large-scale linear modes (Miller, 1986a). The presence of a 1000 m high, 1000 km wide, north-south, Gaussian ridge in the central basin of a three-layer, single-gyre version of this model does not alter the resonant-mode nature of the response. Rough-bottom cases also admit large-scale modal excitation, though typically of reduced amplitude. A sloping-bottom case (see Holland and Schmitz, 1985) allows stronger interior penetration of the model Gulf Stream, thus increasing the nonlinear region of the model. Yet we still find qualitatively similar resonant mode excitation. The ubiquitous presence of this wavelike activity is remarkable.

The eddy-generating region in and around the model Gulf Stream is evidently an effective radiative source for driving a linear open-ocean response. Phillip's (1966) linear ocean, driven by fluctuating winds, was similarly dominated by basin mode resonances which culminated in a broadband peak. (Compare the barotropic meridional velocity spectra in his Figure 1b,c to our meridional velocity spectra in Figures 4e,f and 5e,f.) Harrison (1979) has shown that the amplitude of the broadband peak is sensitive to the bottom friction parameter. Since bottom friction is evidently the response-limiting factor in the present model (see Section 4), a similar conclusion would seem applicable here. In fact, a similar model with only weak Laplacian friction (and no bottom friction) exhibited a monotonous, uncontrolled growth of the most weakly damped (i.e. the grave) linear mode of the system. This supports the notion that the barotropic modes feed on the turbulence until friction limits the response in the far field.

(b) Boundary-current radiation

The linear open-ocean response to localized fluctuating currents in EGCMs was discussed by Harrison and Robinson (1979). Their boundary-forced model was applied to the numerical simulations of Holland (1978) and Robinson *et al.* (1977). They found time and space scales in good agreement with model observed fields in the EGCMs although the frequencies of forcing were necessarily selected *ad hoc* from the diagnosed statistics of the nonlinear region. The response was limited by friction as in the present model. The results of our analysis evidently support their boundary-forcing hypothesis. Note, for example, the relatively well-defined transition in Figure 6d from the higher amplitude, free-jet region to the weaker amplitude, linear basin mode region. Whether the far-field response is simply driven by linear radiation (i.e. boundary-forced by the free-jet region) or whether non-linear resonant interactions occur between modes in the far field (i.e. as in Rhines, 1975; Malanotte-Rizzoli, 1984) has not been shown here; the former, however, appears to be the most plausible explanation due to the relatively low amplitudes of the resonant modes (Table I).

TABLE I

Estimated rms modal amplitudes from the EGCM.

Mode #	(n, m)	Period (days)	$4\pi\sigma_{nm}/\beta$ (km)	rms Amp. (cm)
1	(1, 1)	8.1	5640	0.04
2	(1, 2)	12.8	3570	0.09
3	(2, 1)	12.8	3570	0.24
4	(2, 2)	16.2	2820	0.18
5	(1, 3)	18.1	2520	0.17
6	(3, 1)	18.1	2520	0.45
7	(2, 3)	20.6	2220	0.43
8	(3, 2)	20.6	2220	0.35
10	(4, 1)	23.6	1940	0.65
17	(5, 1)	29.1	1570	1.1
26	(2, 6)	36.2	1260	1.1
34	(7, 1)	40.4	1130	1.9
37	(6, 4)	41.2	1110	0.78

The radiative properties of fully developed unstable waves is not well understood. Haidvogel and Holland (1978) and Holland and Haidvogel (1980, 1981) have shown that instantaneous profiles of EGCM velocity fields (when assumed to be independent of one direction) can support a growing, linearly unstable wave which compares favorably with the space and time scales of the flow. The fact that the growth rate is usually slower than the time scales of variability in the unstable region confounds a simple interpretation. These unstable modes tend to be trapped to the shear region but recent calculations (Holland and Schmitz, 1985) show that radiating modes (Talley, 1983a, b) can also occur although with growth rates which are far slower than any trapped mode.

Does the radiated wave field only provide a mechanism to dissipate the energy of the instabilities of the Gulf Stream region, or can the resonant oscillations, in turn, couple back nonlinearly and lose energy to the turbulence, influencing the space/time scale selection of the unstable, free-jet region? In the small basin case (1000 km square) of Holland (1978), one presumes that the boundaries indeed affect the unstable region. For larger basins, this is probably not true, although the presence of basin mode excitation suggests boundaries may still be important. Perhaps an experiment with absorbing boundaries (modeling the possibly strong dissipative effect of coastal zones) may help answer that question.

(c) Comparison with a wind-forced model

Returning to the question of what drives the open-ocean eddy field, a surprising result is found in Willebrand *et al.*'s (1980) stochastic wind-forced model. Figure 10 shows sea-level, zonal velocity and meridional velocity spectra at station 3 from the present model superposed with analogous mid-ocean spectra extracted from Figure 4 of Willebrand *et al.* The peak amplitude levels are remarkably similar. (Station 2 from the present model exhibits somewhat higher levels.) There is also a parallel in spectral structure, namely resonant mode peaks at high frequencies and a broadband peak at lower frequencies; the models differ in the precise frequencies and amplitudes associated with the peaks. Since the model physics are very similar, the responses depend primarily on the forms of the forcing function and the dissipation, and to some extent the basin

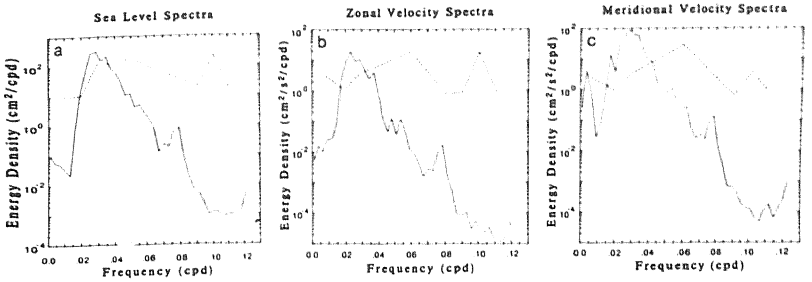

FIGURE 10 Spectra of (a) sea level, (b) zonal velocity, and (c) meridional velocity from (solid lines) station 3 of the present EGCM and (dashed lines) the mid-basin of Willebrand *et al.*'s (1980) stochastic wind-forced model. Spectral levels from the referenced model were extracted directly from their Figure 4. Periods longer than 100 days are excluded. Note the similarity in amplitude for the barotropic broadband peak, centered at about 40 days for the EGCM and about 20 days for the fluctuating wind-driven model. Both models exhibit resonant mode peaks at high frequencies, although the EGCM peaks are typically much weaker. At station 2 (Figures 4b, e and 5b, e), the EGCM broadband peak in energy is about one order of magnitude higher than at station 3.

geometry. The realistic wind field (Willebrand, 1978) of their model and the "realistic" eddy field (cf. Schmitz and Holland, 1982) of the model Gulf Stream apparently are capable of driving quantitatively similar model responses!

The definitive method for distinguishing between these two energy sources for mid-ocean eddies would be through cross-spectra. Theories, however, (e.g. Muller and Frankignoul, 1981) have predicted little or no coherence between atmospheric and oceanic variables for periods between 10 and 100 days. [N.b. Recent observations in the northeast Pacific Ocean by Niiler and Koblinsky (1985) have shown a correlation between barotropic flow and wind-stress curl at periods substantially less than 100 days.] Assuming little coherency in the frequency band of interest, can one ever directly distinguish between intrinsic forcing and direct atmospheric forcing of mid-ocean eddies? Comparing spatial distributions of sea-level variance within frequency bands, as in Figure 6, may prove useful. The major source regions for ocean instabilities are easily identified as western intensified currents. If the wind forcing is also significantly inhomogeneous and distinct from instability source regions, characteristic patterns may arise in observed sea-level spectra as follows.

In the present model, sea-level spectra are red in the high amplitude eddy region near the model Gulf Stream. Away from this region the spectra exhibit a broadband barotropic peak near 40 day period. A spectral gap separates this from the baroclinic activity of periods greater than 150 days. Comparing to Willebrand *et al.*'s (1980) model sea-level spectra (their Figure 4a), a very similar situation occurs. There, the source region appears localized in the north-central part of their basin, and corresponds to the maximum in wind-stress curl amplitude. Away from that region the broadband barotropic peak emerges. If excited barotropic waves are present in the ocean, as in the models, one should be able to detect such variance distributions away from identifiable source regions.

(d) Observability

Is a broadband peak or a spectral gap observed in sea-level spectra? There is an expansive set of sea-level data from Pacific Ocean island tide-gauge stations which is available for analysis (e.g. see Wyrtki, 1979). We note that Luther (1980) observed an excess of power in sea-level spectra in the 35–80 day band in both equatorial and mid-latitude regions. Equatorial response was coherent over large distances and was described as first baroclinic mode Kelvin-wave resonances. Midlatitude regions had responses which were incoherent from island to island and were left unexplained. Barotropic Rossby waves, generated either by fluctuating winds or oceanic instability, could provide an explanation.

As a rudimentary comparison between model and observations, consider Luther's (1982) Figure 10 which shows sea-level spectra from Wake and Eniwetok Islands in the Pacific Ocean. (Note that neither the harmonics of the annual cycle nor inverted barometer effects have been removed. Note also that the ordinate is logarithmic and that energy density is expressed in cm^2/cph in contrast to cm^2/cpd used herein.) Throughout the frequency range the model is deficient in power except for the 25–50 day period band for which levels are comparable to both island stations. A similar conclusion may be drawn for the Atlantic Ocean upon examining the sea-level spectra of Wunsch (1981, p. 352). This is by no means a conclusive comparison. We only suggest that this simple EGCM can produce realistic mid-ocean levels of sea-level variance (albeit in a narrow

band) without particular regard to the choice of parameters other than is necessary for a "realistic" Gulf Stream region response (cf. Schmitz and Holland, 1982; Holland and Schmitz, 1985).

The degree to which real ocean planetary modes may be excited by mesoscale turbulence or atmospheric fluctuations is unknown. Luther's (1982) 5-day, Pacific Ocean oscillation is the only documented clear observation of a resonant planetary mode. He estimates an rms amplitude of 0.4 cm for this atmospheric-pressure-driven wave. Estimates of the rms amplitude of model eddy-excited modes are shown in Table I for some of the fastest oscillations. The grave mode (8 day period) has an rms amplitude of only a few tenths of a mm. In contrast, the resonant 10 day grave mode in Willebrand *et al.*'s (1980) wind-forced model oscillated with about 3 cm rms amplitude. This suggests that larger scale modes will only be weakly excited by radiation from the mesoscale. However, near the barotropic broadband peak (periods greater than about 20 days), typical modal amplitudes are a few cm in the present model. This suggests that smaller-scale, longer period modes may be observable if ocean turbulence behaves in accord with the present model. Excitation may be further enhanced if large-scale topographic features (such as the mid-Atlantic ridge) effectively partition ocean basins into smaller sub-basins (Rhines, 1969; Anderson and Killworth, 1977), thereby confining energy propagation.

6. CONCLUSION

An analysis of a two-layer, flat-bottom EGCM driven by steady wind stress curl in a 4000 km square basin reveals a distinct frequency separation of barotropic and baroclinic motion in the far-field regions removed from strong mean currents. The resultant open-ocean fluctuations are characterized as barotropic (baroclinic) for periods less (greater) than about 100 days. Decomposition of the large-scale barotropic flow reveals the presence of resonantly excited normal modes, evidently driven by the localized instabilities of the free-jet, "Gulf Stream" region. The barotropic open-ocean flow manifests itself as a broadband peak in sea-level spectra between 25 and 50 day periods, comparable in magnitude to observations in that band. The barotropic open-ocean flow is very similar to the

response in Willebrand *et al.*'s (1980) stochastic wind-forced model suggesting the comparable importance of atmospheric and intrinsic forcing of mid-ocean eddies. We suggest that physically motivated, frequency band distributions of sea-level variance derived from the data-base of island tide-gauge stations in the Pacific Ocean may help to distinguish atmospheric from intrinsic forcing of the mid-ocean mesocale eddy field.

The relevance of this extensive wave-like activity to the ocean is not clear. The applicability of QG dynamics (Semtner and Holland, 1978) is supported by favorable comparison with the shallow-water equations model of Willebrand *et al.* (1980). If rough-bottom topography is included in the EGCM, then far-field spectral levels are generally reduced, although the resonant-mode character is unaltered. More elaborate model studies of radiation from strong currents (e.g. Malanotte-Rizzoli, 1984) will help clarify the nature of radiated wave fields and their importance in driving the mid-ocean eddy field. The possibility that western boundary turbulence may excite basin or sub-basin modes motivates further study of topographic and dissipative effects on Rossby modes (e.g. Miller, 1986b).

Acknowledgements

Suggestions from Doug Luther were invaluable in focusing attention on the question of what forces the mid-ocean mesoscale field and on the observational testability of models. The computational expertise of Julianna Chow was greatly appreciated. AJM profited from conversations with Mark Swenson, Rick Salmon, Claude Frankignoul, John Marshall, Annalisa Griffa, Bob Hall, Peter Rhines and Christian LeProvost. The National Science Foundation provided financial support under Grants OCE81-08703 and OCE84-10067 and computer resources through the National Center for Atmospheric Research. This study formed a part of the doctoral dissertation of AJM at the Institute of Geophysics and Planetary Physics of the Scripps Institution of Oceanography.

References

Anderson, D. L. T. and Killworth, P. D., "Spin-up of a stratified ocean, with topography," *Deep-Sea Res.* **24**, 709–732 (1977).

Bretherton, F. P. and Karweit, M., "Mid-ocean mesoscale modeling," *Numerical Models of Ocean Circulation*, Natl. Acad. Sci., 237–295 (1975).

Flierl, G. R., "The application of linear quasi-geostrophic dynamics to Gulf stream rings," *J. Phys. Oceanogr.* **7**, 365–379 (1977).

Flierl, G. R., Kamenkovich, V. and Robinson, A. R., "Gulf Stream meandering and Gulf Stream ring eddy production mechanisms," *Dynamics and the Analysis of Mode-I: Report of the MODE-I Dynamics Group*, Massachusetts Institute of Technology, Cambridge, Massachusetts, 113–135 (1975).

Gill, A. E., Green, J. S. A. and Simmons, A. J., "Energy partition in the large-scale ocean circulation and the production of mid-ocean eddies," *Deep-Sea Res.* **21,** 499–528 (1974).

Haidvogel, D. B. and Holland, W. R., "The stability of ocean currents in eddy resolving general circulation models," *J. Phys. Oceanogr.* **8,** 393–413 (1978).

Haidvogel, D. B. and Rhines, P. B., "Waves and circulation driven by oscillatory winds in an idealized ocean basin," *Geophys. & Astrophys. Fluid Dyn.* **25,** 1–63 (1983).

Harrison, D. E., "On the linear equilibrium basin response to fluctuating winds, and mesoscale motions in the ocean," *J. Geophys. Res.* **84,** 1221–1224 (1979).

Harrison, D. E. and Holland, W. R., "Regional eddy vorticity transport and the equilibrium vorticity budgets of a numerical model ocean circulation," *J. Phys. Oceanogr.* **11,** 190–208 (1981).

Harrison, D. E. and Robinson, A. R., "Energy analysis of open regions of turbulent flows—mean eddy energetics of a numerical ocean circulation experiment," *Dyn. Atmos. & Oceans* **2,** 185–211 (1978).

Harrison, D. E. and Robinson, A. R., "Boundary-forced planetary waves: A simple model mid-ocean response to strong current variability," *J. Phys. Oceanogr.* **9,** 919–929 (1979).

Holland, W. R., "The role of mesoscale eddies in the general circulation of the ocean—numerical experiments using a wind-driven quasi-geostrophic model," *J. Phys. Oceanogr.* **8,** 363–392 (1978).

Holland, W. R. and Haidvogel, D. B., "A parameter study of the mixed instability of idealized ocean currents," *Dyn. Atmos. & Oceans* **4,** 185–215 (1980).

Holland, W. R. and Haidvogel, D. B., "On the vacillation of an unstable baroclinic wave field in an eddy-resolving model of the ocean general circulation," *J. Phys. Oceanogr.* **11,** 557–568 (1981).

Holland, W. R., Harrison, D. E. and Semtner, A. J. Jr., "Eddy-resolving models of large-scale ocean circulation," *Eddies in Marine Science*, Springer-Verlag, Berlin, 379–403 (1983).

Holland, W. R. and Rhines, P. B., "An example of eddy-induced mean oceanic circulation," *J. Phys. Oceanogr.* **10,** 1010–1031 (1980).

Holland, W. R. and Schmitz, W. J., "On the zonal penetration scale of model mid-latitude jets," *J. Phys. Oceanogr.* **15,** 1859–1875 (1985).

Luther, D. S., *Observations of Long Period Waves in the Tropical Ocean and Atmosphere*, Ph.D. dissertation, Massachusetts Institute of Technology and the Woods Hole Oceanographic Institution, 210 pp. (1980).

Luther, D. S., "Evidence of a 4–6 day, barotropic, planetary oscillation of the Pacific Ocean," *J. Phys. Oceanogr.* **12,** 644–657 (1982).

Malanotte-Rizzoli, P., "Boundary-forced nonlinear planetary radiation," *J. Phys. Oceanogr.* **14,** 1032–1046 (1984).

Miller, A. J., *Barotropic Planetary-Topographic Oscillations in Ocean Basins*, Ph.D. dissertation, Scripps Institution of Oceanography, University of California, San Diego, 133 pp. (1986a).

Miller, A. J., "Non-divergent planetary oscillations in mid-latitude ocean basins with continental shelves", accepted by *J. Phys. Oceanogr.* (1986b).

Muller, P., "Evidence for the direct atmospheric forcing of mid-ocean eddies," *Proceedings, 'Aha Huliko'a Hawaiian Winter Workshop*, University of Hawaii, January 5–7, 1983, Hawaii Institute of Geophysics, 113–127 (1983).

Muller, P. and Frankignoul, C., "Direct atmospheric forcing of geostrophic eddies," *J. Phys. Oceanogr.* **11,** 287–308 (1981).

Niiler, P. P. and Koblinsky, C. J., "A local time-dependent Sverdrup balance in the eastern North Pacific Ocean," *Science* **229,** 754–756 (1985).

Pedlosky, J., "A study of the time-dependent ocean circulation," *J. Atmos. Sci.* **22,** 267–272 (1965).

Pedlosky, J., "Fluctuating winds and the ocean circulation," *Tellus* **19,** 250–256 (1967).

Pedlosky, J., "On the radiation of meso-scale energy of the mid-ocean," *Deep-Sea Res.* **24,** 591–600 (1977).

Pedlosky, J., *Geophysical Fluid Dynamics*, Springer-Verlag, New York, (1979).

Phillips, N. A., "Large-scale eddy motion in the western Atlantic," *J. Geophys. Res.* **71,** 3883–3891 (1966).

Rhines, P. B., "Slow oscillations in an ocean of varying depth. Part I. Abrupt topography," *J. Fluid Mech.* **37,** 161–189 (1969).

Rhines, P. B., "Waves and turbulence on a beta-plane," *J. Fluid Mech.* **69,** 417–443 (1975).

Rhines, P. B., "The dynamics of unsteady currents," *The Sea, Volume 6, Marine Modelling*, Wiley, New York, 189–318 (1977).

Rhines, P. B. and Bretherton, F. P., "Topographic Rossby waves in a rough-bottomed ocean," *J. Fluid Mech.* **61,** 583–607 (1973).

Robinson, A. R., ed., *Eddies in Marine Science*, Springer-Verlag, Berlin, (1983).

Robinson, A. R., Harrison, D. E., Mintz, Y. and Semtner, A. J., "Eddies and the general circulation of an idealized oceanic gyre: A wind and thermally driven primitive equation numerical experiment," *J. Phys. Oceanogr.* **7,** 182–207 (1977).

Robinson, A. R. and McWilliams, J. C., "The baroclinic instability of the open ocean," *J. Phys. Oceanogr.* **4,** 281–294 (1974).

Schmitz, W. J., and Holland, W. R., "A preliminary comparison of selected numerical eddy-resolving general circulation experiments with observations," *J. Mar. Res.* **40,** 75–117 (1982).

Semtner, A., and Holland, W. R., "Intercomparison of quasigeostrophic simulations of the western North Atlantic circulation with primitive equation results," *J. Phys. Oceanogr.* **8,** 735–754 (1978).

Talley, L. D., "Radiating barotropic instability," *J. Phys. Oceanogr.* **13,** 972–987 (1983a).

Talley, L. D., "Radiating instabilities of thin baroclinic jets," *J. Phys. Oceanogr.* **13,** 2161–2181 (1983b).

Willebrand, J., "Temporal and spatial scales of the wind field over the North Pacific and North Atlantic," *J. Phys. Oceanogr.* **8,** 1080–1093 (1978).

Willebrand, J., Philander, S. G. H. and Pacanowski, R. C., "The oceanic response to large-scale atmospheric disturbances," *J. Phys. Oceanogr.* **10,** 411–429 (1980).

Wunsch, C., "Low frequency variability of the sea," *Evolution of Physical Oceanography*, MIT Press, Cambridge, Massachusetts, 342–374 (1981).

Wyrtki, K., "Sea level variations: monitoring the breadth of the Pacific," *EOS, Trans. Am. Geophys. Union* **60,** 25–27 (1979).